Evaluation of the printability of agar and hydroxypropyl methylcellulose gels as gummy formulations: Insights from rheological properties

Morenikeji Aina, Fabien Baillon, Romain Sescousse, Noelia M. Sanchez-Ballester, Sylvie Begu, Ian Soulairol, Martial Sauceau

▶ **To cite this version:**

Morenikeji Aina, Fabien Baillon, Romain Sescousse, Noelia M. Sanchez-Ballester, Sylvie Begu, et al.. Evaluation of the printability of agar and hydroxypropyl methylcellulose gels as gummy formulations: Insights from rheological properties. International Journal of Pharmaceutics, 2024, 654, pp.123937. 10.1016/j.ijpharm.2024.123937 . hal-04490142

HAL Id: hal-04490142

https://imt-mines-albi.hal.science/hal-04490142

Submitted on 5 Mar 2024

HAL is a multi-disciplinary open access archive for the deposit and dissemination of scientific research documents, whether they are published or not. The documents may come from teaching and research institutions in France or abroad, or from public or private research centers.

L'archive ouverte pluridisciplinaire **HAL**, est destinée au dépôt et à la diffusion de documents scientifiques de niveau recherche, publiés ou non, émanant des établissements d'enseignement et de recherche français ou étrangers, des laboratoires publics ou privés.

Distributed under a Creative Commons Attribution 4.0 International License

International Journal of Pharmaceutics 654 (2024) 123937

Contents lists available at ScienceDirect

International Journal of Pharmaceutics

journal homepage: www.elsevier.com/locate/ijpharm

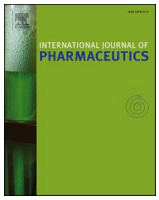

Evaluation of the printability of agar and hydroxypropyl methylcellulose gels as gummy formulations: Insights from rheological properties

Morenikeji Aina [a,*], Fabien Baillon [a], Romain Sescousse [a], Noelia M Sanchez-ballester [b,c], Sylvie Begu [b], Ian Soulairol [b,c], Martial Sauceau [a]

[a] RAPSODEE, IMT Mines Albi, CNRS, University of Toulouse, 81013 Albi, France
[b] ICGM, University of Montpellier, CNRS, ENSCM, Montpellier, France
[c] Department of Pharmacy, Nîmes University Hospital, Nîmes, France

ARTICLE INFO

Keywords:
gels
drug delivery
rheology
printability
extrusion 3D printing
principal component analysis (PCA)

ABSTRACT

The trial-and-error method currently used to create formulations with excellent printability demands considerable time and resources, primarily due to the increasing number of variables involved. Rheology serves as a relatively rapid and highly beneficial method for assessing materials and evaluating their effectiveness as 3D constructs. However, the data obtained can be overwhelming, especially for users lacking experience in this field. This study examined the rheological properties of formulations of agar, hydroxypropyl methylcellulose, and the model drug caffeine, alongside exploring their printability as gummy formulations. The gels' rheological properties were characterized using oscillatory and rotational experiments. The correlation between these gels' rheological properties and their printability was established, and three clusters were formed based on the rheological properties and printability of the samples using principal component analysis. Furthermore, the printability was predicted using the sample's rheological property that correlated most with printability, the phase angle δ, and the regression models resulted in an accuracy of over 80 %. Although these relationships merit confirmation in later studies, this study suggests a quantitative definition of the relationship between printability and one rheological property and can be used for the development of formulations destined for extrusion 3D printing.

1. Introduction

Additive manufacturing, commonly referred to as 3D printing (3DP), is a technology that uses one or more materials to build a solid object in a layer-by-layer manner from a digital model using a 3D printer (Shen et al., 2022). These 3D printers could also be made available anywhere, making on-demand printing possible, and could prove useful in time- or resource-constrained settings such as disaster areas, during pandemics, in emergency or operating rooms (Bhutani et al., 2021; Hsiao et al., 2020; Miller et al., 2022). 3D printing has unique advantages in pharmaceutics for preparing tailored dose formulations with special or customized shapes (Alqahtani et al., 2023; Herrada-Manchon et al., 2020; Tracy et al., 2023), release profiles (Cailleaux et al., 2021; Tabriz et al., 2023) and/or personalized doses (dos Santos et al., 2023). This can solve the problem encountered in neonatal pharmacotherapy, where the administration of the right dose of drugs is required due to the differences in the physiology of neonates. These differences affect drug pharmacokinetics, thus, making the extrapolation of dosages from adults and older children inappropriate. 3D printing can thus not only solve the problem of dysphagia among patients (Herrada-Manchon et al., 2020; Karavasili et al., 2022; Panraksa et al., 2022) but also improve the drug's dissolution and/or disintegration due to the porous nature of the printed drug (Boudriau et al., 2016; Panraksa et al., 2022) thereby improving medication adherence.

In semi-solid extrusion (SSE), a 3DP technique, the material (usually semi-solid such as gels or pastes) is deposited in sequential layers to create the 3D object. Since these gels or pastes are mainly composed of water, print quality can ultimately be hindered, and therein lies the problem associated with SSE. This is especially critical for objects destined for pharmaceutical applications, where it is essential to produce highly accurate and reproducible 3D printed constructs, thereby reducing dose variations, and improving the visual appearance of the object and ultimately its acceptance by the end-user and the regulatory body. To explain further, the extruded material should produce smooth

* Corresponding author.
E-mail address: morenikeji.aina@mines-albi.fr (M. Aina).

https://doi.org/10.1016/j.ijpharm.2024.123937
Received 13 December 2023; Received in revised form 20 February 2024; Accepted 21 February 2024
Available online 23 February 2024
0378-5173/© 2024 The Author(s). Published by Elsevier B.V. This is an open access article under the CC BY license (http://creativecommons.org/licenses/by/4.0/).

and uniform filaments within the range of the 3D printer's pressure specification (extrudability), and, the lowest layer should be able to support the upper layers (shape retention) (Mu et al., 2023; Zhu et al., 2023; Zidan et al., 2019), thus reducing dimension and weight variability. One of the methods used to evaluate the print quality of objects semi-quantitatively is "printability". It is defined as the ability of materials to achieve extrusion and maintain shape fidelity with high printing accuracy, depending on the 3D printer type (Bom et al., 2022).

Hydroxypropyl methylcellulose (HPMC) and agar are polysaccharides that are widely implemented in the food and pharmaceutical field, as gelling agents (Jeong et al., 2012). HPMC is a cellulose derivative whose aqueous solution undergoes sol–gel transition around 80 °C (Joshi, 2011) and is obtained through the substitution of hydroxyl groups on the cellulose chain with methoxy and hydroxypropyl groups (Perez-Robles et al., 2022). Agar, on the other hand, is composed of agarose and agaropectin with the former responsible for gelation. It is soluble in water at temperatures between 95 and 100 °C and undergoes sol–gel transition under 40 °C (Mao et al., 2016, 2017). Several studies have reported the use of HPMC alone (Cheng et al., 2020; Polamaplly et al., 2019) or combined with other materials for SSE (Heckl et al., 2023; Tagami et al., 2019; H. S. Yang & Kim, 2023). For example in the study of H. S. Yang & Kim, (2023), the authors reported the use of 5 to 20 % w/w HPMC. They observed that at room temperature (RT) and low pressure, the extrudability of low concentration of HPMC was good but the printed tablets had poor shape retention. On the contrary, high concentrations of HPMC resulted in better shape retention but poorer extrudability (even at a high printing pressure), due to the material's high viscosity (H. S. Yang & Kim, 2023). The same observations were reported for agar gels, whose high viscosity made it difficult to be printed at RT (Wei et al., 2015), rendering it only extrudable at higher temperatures (Kamlow et al., 2021) or when mixed in small quantities with other polymers (Rahman et al., 2020; Wang et al., 2021). It should be noted that the thickening/binding function of HPMC promotes the formation of uniform and smooth printing filaments (Mora-Castaño et al., 2022), while the high viscosity of agar is beneficial in maintaining the shape of the extruded sample.

One characterization technique that has often linked the extrudability and shape retention abilities of materials to their "printability" in SSE is rheology (Liu et al., 2019; Temirel et al., 2022). Although rheology provides valuable information about a material's flow properties, the information can be overwhelming, particularly for inexperienced users. As with large dimensions of data, it is challenging to discern patterns and would require years of experience, and to date, there is still misinformation and a lack of uniformity of concepts and analysis methodologies to be adopted. Researchers perform different rheological measurements, from traditional viscosity measurements to more advanced oscillatory amplitude shear studies (Elbadawi et al., 2020). Furthermore, despite the correlation of the rheological properties of materials to their feasibility for SSE (Bom et al., 2022), there is still a lack of knowledge on what limits and parameters can be set as references, and how to screen the materials (Firth et al., 2018). Studies have also shown that the process involved in extrusion printing requires materials with unique and somehow contradictory rheological performances (Ainis et al., 2023) making it imperative to have a balance between the rheological requirements for extrusion and shape retention. For example, if a gel with low yield stress is used to help extrusion stages, then the extruded sample will not retain its shape. On the contrary, if stiff gels with high yield stress and viscosity are used for attaining shape retention, then it will increase the required extrusion force, and extrusion through the nozzle will be difficult (Bom et al., 2022). In addition, drug loading exceeds the drug solubility in high-dose formulations, resulting in formulations containing solid drug particles (Teoh et al., 2022). These solid particles (being either the drug or the excipients) affect the rheological and subsequently, the flow properties of the paste/gel (Genovese et al., 2007; Teoh et al., 2022) and the effects of these solid particulates on the printing process and printability have also not been systemically investigated in the literature.

A complete rheological evaluation, however, neither defines absolute criteria nor quantitative limits for printability as well as the measured rheological parameters. This could be because of the existence of great complexity and variety of printable materials as well as printing approaches and the fact that rheological evaluations display material properties at a defined condition (e.g., at rest, during printing, after preshear). Nevertheless, we believe that the evaluations demonstrated in this work can contribute to the understanding of what parameters govern printability and assist in the choice of the rheological test to perform for the effective optimisation of materials destined for use in semi-solid extrusion. Notably, to the best of our knowledge, there is no report on the combination of the thickening/binding function of HPMC with the high viscosity of agar to produce extrudable and self-supporting gels. We thus, investigated the rheological properties of agar gels (A) and agar-HPMC (AH) gels at increasing HPMC concentrations as well as samples containing sucrose and caffeine (for formulations destined for drug delivery purposes). We also correlated the rheological properties of the formulations with their 3D printing behaviour. Finally, principal component analysis (PCA) was performed to explain the correlation between the rheological properties and the printability, and prediction models for the printability were obtained.

2. Material and method

2.1. Materials

All materials used in the different formulations were pharmaceutical grade: Agar (A), pulverised sucrose (S), and anhydrous caffeine (C) were purchased from Cooper's Laboratory, France, and Methocel K4M (HPMC, H) (USP 2208 grade, 4000 cp, Controlled release (CR) Premium, MW = 2.1 × 105 g/mol, 8.1 % hydroxypropyl and 22 % methoxy substituted) was obtained as a gift from Colorcon Ltd, France. All the samples were prepared with deionized water obtained with Aquadem® water demineraliser (Veolia Waters Technology, France).

2.2. Preparation of hydrogels

Hydrogels were prepared by mixing A, H, S, and C in deionized water in the proportions (in % w/w) as shown in Table 1. Briefly, the powders were weighed and placed in a beaker after which, they were mixed to ensure proper homogenization using a stainless-steel laboratory spatula. While stirring, deionized water heated to 98 °C was slowly added to the homogenized powder mixture. After a lump-free paste was formed, the beaker containing the paste was placed in a water bath at 95 °C until an amber or white-coloured solution was formed. This solution was then

Table 1
Sample notation and aqueous composition (in % w/w).

Notation	A	H	S	C
3A	3	–	–	–
3A2H	3	2	–	–
3A3H	3	3	–	–
3A4H	3	4	–	–
3A5H	3	5	–	–
4A	4	–	–	–
4A2H	4	2	–	–
4A3H	4	3	–	–
4A4H	4	4	–	–
4A5H	4	5	–	–
10S0C	3	2	10	–
10S1C	3	2	10	1
10S2C	3	2	10	2
10S3C	3	2	10	3
10S5C	3	2	10	5
10S7C	3	2	10	7
10S10C	3	2	10	10

left at RT (T = 20 °C) overnight before rheological analysis and 3D printing. The concentrations of agar used (3 and 4 %) were selected based on preliminary assessments, these samples on their own possessed good shape retention but poor extrudability. Also based on preliminary assessments, we chose the concentrations of HPMC (2 – 5 %) to study their effect on the extrudability of the agar gels. For the formulations destined for drug loading of caffeine, 10 % sucrose was added to improve the palatability of the formulation as demonstrated in the study by Tang et al., (2017) on the improvement of the palatability of mefloquine, a strongly bitter active pharmaceutical ingredient (API).

2.3. Rheological analysis

Rheological measurements can be performed using rotational or oscillatory tests (D. Yang et al., 2020). In oscillation measurements, the sample is placed in between two plates. Sinusoidal movements (of one of the plates) on the tested sample, provide information on the equilibrium structure of the sample, which can then be used to determine the viscoelasticity of materials. For rotational rheological measurements, the response of the sample to the rotational movement of one of the plates at defined speeds can be used to provide information on flowability (Cheng et al., 2022; TA Instruments, n.d.). The rheological behaviour of the formed gels/pastes was investigated using a Thermo-Haake RheoStress 600 (RS600) rheometer. Plate–plate geometry (diameter = 35 mm) was used and a gap height between 0.1 and 0.5 mm was set based on the sample and the test being performed. All measurements were performed in duplicates and conducted at 20 °C.

2.3.1. Oscillation test

Information on the viscoelastic behaviour of the samples was obtained through oscillatory tests. First, the linear viscoelastic region (LVER) was located under controlled stress mode, in this region, tests can be conducted without destroying the sample's structure. Next, a steady stress of 30 Pa (in the LVER) was applied for 30 s, followed by an equilibration for 30 s to erase the sample history. The frequency sweep was then conducted from 0.1 to 10 Hz at 30 Pa. The exponent (m, dimensionless) was obtained from fitting the elastic/storage modulus (G' in Pa) as a function of the frequency (f in Hz) to a power law equation. The phase angle (δ in °) is the inverse tangent of viscous modulus (G'') to G' ratio and ranges from 0° (elastomeric solid) and 90° (viscous liquid) (Baumgardner et al., 2007). The G', G'', and δ were taken at plateau values in the LVER of the oscillation sweep from 1 to 1000 Pa at 1 Hz. The critical strain (γ_c, %) and yield point (τ_c, Pa) were defined as the strain and stress, respectively at the end of the LVER (±10 % deviation; according to ASTM D7175 and DIN 51810–2). The change in elastic modulus (CEM) was defined as the difference between the G' at the end of the LVER and the G' at the end of the analysis (at 1000 Pa).

2.3.2. Rotation test

Flow curves were obtained through rotational tests in which the shear rate was reduced stepwise from 1 to $10e^{-02}$ s^{-1} on a logarithmic scale with 10 s per data point. The samples were also pre-sheared at 10 s^{-1} for 30 s and equilibrated for 30 s before all measurements were taken. Since all samples were solids at RT, their true yield stress (τ_y, in Pa) could not be measured, but instead, they were quantified, together with other rheological parameters (plastic viscosity - μ_p in Pa.s, consistency index - K in Pa.s^n and flow index - n unitless), using Casson and Ostwald-de Waele Power Law model (equations (1) and (2) respectively)

$$\tau^{0.5} = \tau_y{}^{0.5} + \left(\mu_p \dot{\gamma}\right)^{0.5} \quad (1)$$

$$\tau = K\dot{\gamma}^n \quad (2)$$

2.4. Printability assessment

In this study, we used the semi-quantitative method developed by Ouyang et al., (2016) to evaluate the printability based on the gelation degree. This parameter is influenced by pre-printing (rheological and nozzle features), printing (e.g., object design, pressure, temperature, flow rate, environmental conditions), and post-printing parameters (e.g., crosslinking or drying techniques) (Bom et al., 2022). The printability assessment of the gels was performed at RT. A pneumatic 3D Printer (Delta WASP 2040, Italy) was used to print a 4.6 mm x 4.6 mm square grid with 4 layers using a 0.8 mm nozzle diameter. The printing speed was set at 20 mm/s and the extrusion pressure was between 4 and 5 bar. To determine the printability, (*Pr*, unitless) value of each sample, optical images of printed squares were analysed in ImageJ to determine their perimeter, L, and area, A (n = 5). The *Pr* was calculated using equation (3). In ideal conditions, the *Pr* is equal to 1, representing proper gelation conditions, smooth and uniform filaments are extruded continuously with clearly distinguished layers. However, the printing of under-gelled samples ($Pr < 1$) results in fused layers with poor mechanical strength whereas the printing of over-gelled samples ($Pr > 1$) results in irregular filaments with fractured morphology. For extrusion purposes, *Pr* values between 0.9 and 1.1 have been demonstrated to have good extrudability and shape retention ability (Ouyang et al., 2016). However, in this study, we considered the range for good printability to be between 0.94 and 1.14. Samples with printability lower than 0.94 had poorer shape fidelity and required post-treatment ("Under-gelled") whereas samples with $Pr > 1.14$ were hard to extrude and had poor ductility ("Over-gelled").

$$Pr = \frac{L^2}{16A} \quad (3)$$

2.5. Data analysis

Spearman rank-order correlation matrix and the linkage according to hierarchical cluster analysis of Spearman's correlations were built to understand the relationship between rheological parameters and printability of A and AH gels. Next, principal component analysis (PCA) was used to identify clusters based on the sample's rheological properties. The rheological data were first mean-centred and scaled to the variance. The matrix was then decomposed into principal components (PCs) by applying singular vector decomposition (SVD). The evaluation was performed by plotting the matrix of the factor loadings and plotting all the scores of the components whose variance is greater than the average variance of all the PCs. It should be highlighted that the scores of the samples containing caffeine and sucrose were determined using the coefficient obtained from the SVD. Non-linear predictive models were built with the printability and the rheological parameter(s) that had the best correlation with the printability. The predictive performance was evaluated using the regression coefficient (R^2Y) and the residual prediction deviation (RPD) from the regression model and the actual 3D printing data (equations (4) and (5). An R^2Y value between 0.66 and 0.81 indicates that the model can be used for screening, values between 0.83 and 0.90 indicate that the model is usable with caution for most applications, whereas values between 0.92 and 0.96 indicate that the model is usable in quality assurance. A RPD value between 2.5 and 2.9 indicates that the model can be used for screening while values between 3.0 and 3.4 indicate that the model can be used for quality control (Onsawai et al., 2021).

$$R^2Y = \frac{\sum_{i=1}^{N}(\hat{y}_i - \bar{y})^2}{\sum_{i=1}^{N}(y_i - \bar{y})^2} \quad (4)$$

$$RPD = \sqrt{\frac{\sum_{i=1}^{N}(y_i - \bar{y})^2}{\sum_{i=1}^{N}(\hat{y}_i - y_i)^2}} \quad (5)$$

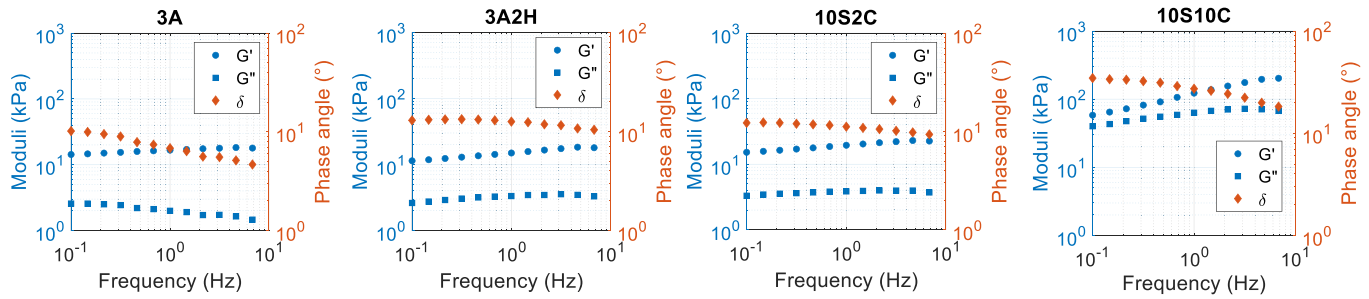

Fig. 1. G', G'' and δ as a function of frequency at 20 °C of selected samples.

3. Results

3.1. Oscillation frequency sweep

Fig. 1 shows the dynamic moduli for all considered material compositions at RT as a function of frequency. All samples presented clear viscoelastic behaviour with the G' and G'' suggesting solid-like (elastic) and fluid-like (viscous) properties, respectively (Cheng et al., 2022; Cofelice et al., 2023). The G' of AH gels increased with the oscillation frequency, indicating that the samples were weak gels at 20 °C, but the A gels displayed lower dependence, and could thus be classified as physical gels with well-structured systems (Gu et al., 2017; Nobile et al., 2008). Furthermore, at any oscillation frequency, the A gels exhibited more elastic properties than the AH gels, suggesting that the A gels present a more solid-like behaviour at a high deformation rate, which may hinder the flowability of the materials during the printing process (Tejada-Ortigoza & Cuan-Urquizo, 2022). In addition, the G" of A gels decreased with increasing frequency, whereas the addition of HPMC to the A gels resulted in a higher G" that increased with increasing frequency. This implies that while all the samples behave as a viscoelastic solid during printing (fast event/high frequency), the AH gels had more tendency to flow like a viscoelastic liquid at rest (slow event/very low frequency) (Rheology Testing Services, n.d.).

Results also show that the phase angles of A gels decreased greatly with increasing frequency compared to AH gels, which showed smaller variations with frequency. Similarly, the addition of 2H to the A gels resulted in an increase of over 40 % in the phase angle, after which the addition of more HPMC only resulted in a slight increase, further demonstrating an increase in the viscous properties of the AH gels. It was also observed that the response of samples containing sucrose and dissolved caffeine (e.g. 10S10C) to a frequency sweep was more like the AH gels than to the A gels. In contrast, samples containing undissolved caffeine (10S3C and above) exhibited responses that were more like A gels than AH gels. These samples also displayed a more frequency-dependent behaviour, commonly observed in suspensions (Nasu & Otsubo, 2006), with the G' and G'' possibly approaching a cross-over point at lower frequencies (more tendency to flow as a viscoelastic liquid at rest than the AH gels).

The exponent, m varies between 0 (elastomeric solid) and 2 (classical liquid) and can be used to distinguish between formulations containing different concentrations of the same polymer from formulations containing different polymers (Gholamipour-Shirazi et al., 2019). Fig. 2a shows that the power law exponent of A gels was lower than 0.1, indicating the existence of a cross-linked elastomer (Chile et al., 2017). The m of AH gels ranged from 0.1 to 0.2, increasing with the concentration of HPMC added. This can be explained by the less dense network formed by the hydration shells around the HPMC molecules during its dissolution in water (Georgopoulos et al., 2004; Liu et al., 2008). Gels with an m-index between 0.03 and 0.13 show good shape retention after printing (Gholamipour-Shirazi et al., 2019), it can thus be inferred that A and AH gels containing 2H should display good shape retention abilities as well as good extrudability. Furthermore, we expected an increase in rheological parameters (e.g. m-index) after the addition of 10 % sucrose (the taste masking agent) and caffeine (the active). It was therefore more prudent to use the 3A2H gel for drug loading as it was more pertinent for us to be able to conduct printability studies of the drug-loaded formulations. Results of the m index on adding sucrose to 3A2H gels (10S0C) and loading caffeine to 10S0C gels are presented in Fig. 2b. Here we see that the 10S0C gel resulted in a slightly lower m index when compared to 3A2H gels (0.09 vs 0.11) whereas the addition of caffeine to 10S0C gel resulted in a slight change until the addition of 3 % caffeine, after which a greater increase of the m index was observed. This could be attributed to the insoluble caffeine aggregates (solubility of caffeine is about 2.2 % at RT (Spiller, 1997) acting as inactive fillers and weakening the gel structure as well as fluidifying the gel (Dille et al., 2015; Klost et al., 2020). In these samples, G' was more dependent on frequency because of the relaxation processes that occurred at short time scales, characteristic of a less gelled system (Lizarraga et al., 2006).

3.2. Oscillation amplitude sweep

Generally, the mechanical strength of materials is reflected by the G' and materials with good mechanical strength possess better resistance to deformation and can therefore be considered to exhibit good self-supporting properties (Liu et al., 2020). However, as highlighted in the study by Townsend et al., (2019) materials with a higher viscous flow will flow until their mechanical energy is fully dissipated whereas those that are strongly elastic will show brittle fracture during flow. It is therefore preferable for printable gels to possess an adequate balance between elastic and viscous behaviour. The G' and G'' of selected samples as a function of the imposed stress is shown in Fig. 3. We observed that all samples (e.g. 3A, 3A2H and 10S2C) showed similar curves (except samples containing 3C and above), displaying the behaviour of a weak strain overshoot of G'' (Type III network) (Bi et al., 2017; Hyun et al., 2002). For this type of network, the loss term becomes dominant at larger strain amplitudes leading to the strain thinning and the overshoot may be regarded as the result of the balance between the formation and the destruction of network junctions (Sim et al., 2003). This overshoot, however, decreased with the addition of other polymers (as observed for 3A2H and 10S2C samples) possibly due to the addition of more interaction sites which aided in the formation of anisotropic structures (Feroz & Dias, 2021). On the other hand, samples containing undissolved caffeine (e.g. 10S10C) displayed strain-thinning behaviour (Type I network) which is commonly observed in suspensions. In systems like this, the polymer chains disentangle and flow more readily as the strain increases (Hyun et al., 2002).

Fig. 4a and b show that G' and G'' increased with the agar concentration and the values of 4AH gels were always higher than those of 3AH gels. The G' of AH gels, however, decreased with the increase of H while the G'' increased. From Fig. 4c, δ was observed to steadily increase with

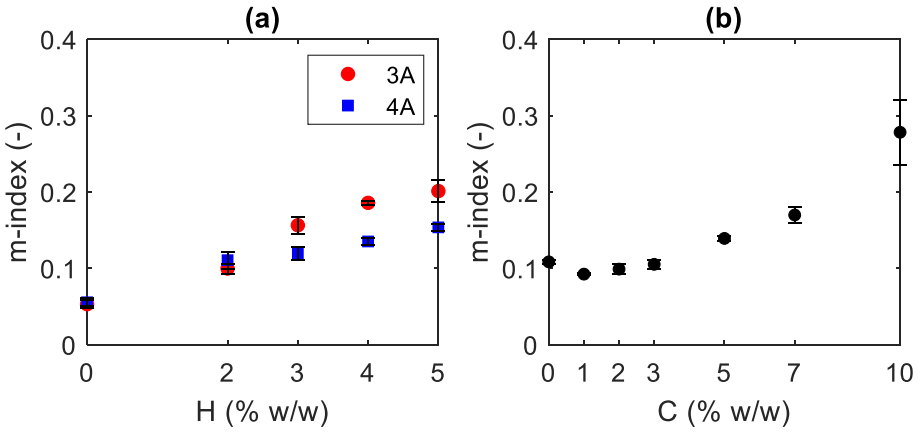

Fig. 2. Power law exponent m of the frequency sweep for (a) A and AH gels (b) 10S gels of different caffeine concentrations. Error bars are standard deviations based on duplicate experiments.

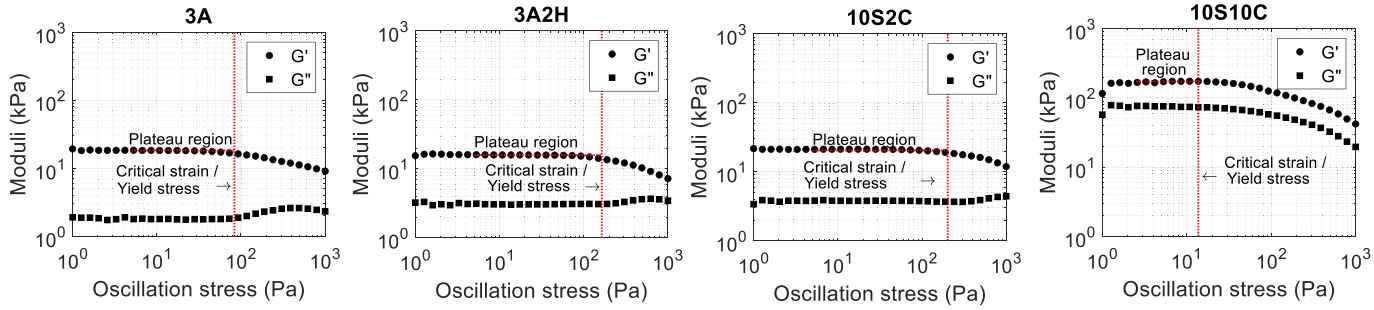

Fig. 3. G' and G'' as a function of oscillation stress showing the end of the LVER of selected samples.

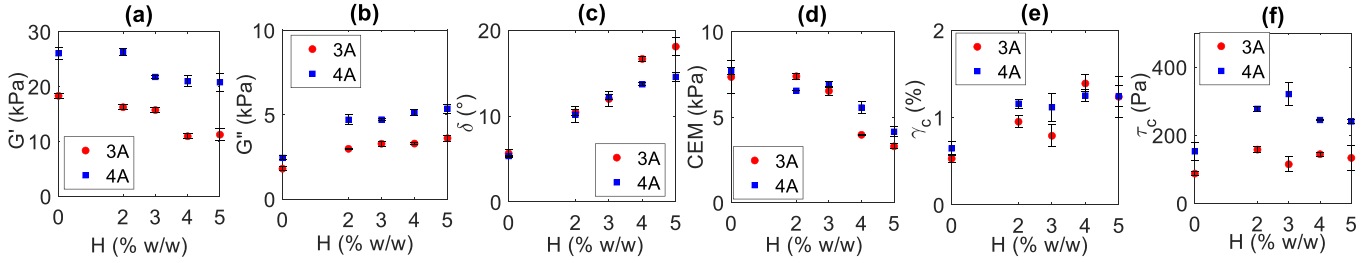

Fig. 4. (a) G', (b) G'' and (c) δ in the LVER, (d) CEM (e) γ_c (f) τ_c of A and AH gels. Error bars are standard deviations based on duplicate experiments.

increasing HPMC concentration. On the other hand, CEM decreased with increasing HPMC concentration showing a similar trend for AH gels containing 3A and 4A (Fig. 4d). From Fig. 4e & f, γ_c and τ_c generally increased with the addition of H. These observations could be a result of the thickening as well as the binding ability of HPMC (R. Varges et al., 2019; Vandevivere et al., 2020). The lower G' indicates that the cross-linking density of the hydrogel network exhibits an order from high to low with increasing HPMC concentration, leading to a decrease in supporting ability. The higher G'' and δ, in contrast, translate to samples with better extrudability (GhavamiNejad et al., 2020). Furthermore, brittle fracturing (commonly observed in stiff materials) is associated with a sharp drop of the G' (higher CEM) whereas a gradual change or

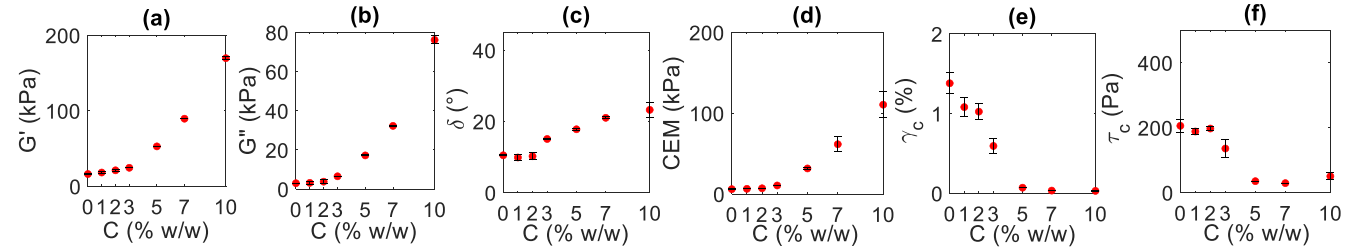

Fig. 5. (a) G', (b) G'' and (c) δ in the LVER, (d) CEM (e) γ_c (f) τ_c of 10S gels of different caffeine concentrations. Error bars are standard deviations based on duplicate experiments.

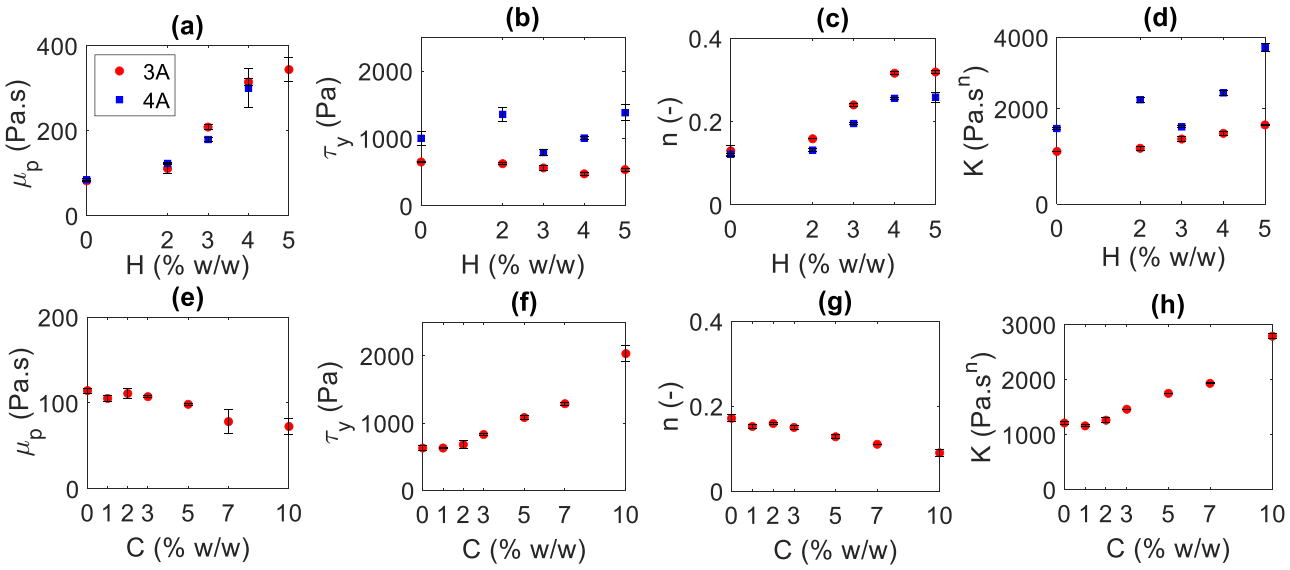

Fig. 6. μ_p, τ_y, n and K of A and AH gels of different HPMC concentrations (a-d) and 10S of different caffeine concentrations (e-h). Error bars are standard deviations based on duplicate experiments.

decrease indicates a ductile fracture (Anton Paar, n.d.), it can, thus be said that AH gels have better ductility than A gels. Regarding τ_c and γ_c, higher values are mostly desirable since that translates to better shape retention and ductility, respectively (Mouser et al., 2016).

From Fig. 5a-f, G', G'', δ and CEM only increased after the addition of 3C or more whereas a decrease of γ_c and τ_c was observed with increasing caffeine concentration. These results demonstrate that the network synergy between the polymers is not purely additive. For 10S10C, whose G' is the highest, the greater number of particles in the gels likely produced an increased resistance to flow and increased particle–particle interaction which led to higher mechanical strength (Teoh et al., 2022). However, their higher phase angle suggests a less gelled network, possibly through the inhibition of the interactions of the gelling systems (agar and HPMC) by the large number of caffeine particles present. Furthermore, it can be inferred that formulations containing 3C and above, deviated from solid gels to colloidal suspensions (Deb et al., 2018) since increasing caffeine concentration reduced the γ_c to the order of 10^{-2} % (El Bitouri, 2023) as well as increased fluid-like properties (increase in δ). In addition, γ_c has been reported to be inversely proportional to the solid character of the sample (Herrada-Manchón et al., 2022) where samples with lower G' permit the elongation of the structural network under continually increasing straining force before eventually deforming and reaching the limit of linearity (as observed in A and AH gels). On the contrary, for samples containing 3C and above, the higher G' did not permit the elongation of the structural network, and the yield point was observed to be inversely proportional to the solid character of the sample. Interestingly, the CEM for the colloidal suspensions was observed to be much higher even though the samples had greater ductility. We believe that the end of the LVER observed in these samples, highlights minute changes in the particle-particle contacts such as the breakage of small range interparticle bonds, and therefore, does not mean that the system starts to flow. In contrast, the values observed for A and AH gels are more related to the actual reorganization of the particle network at flow onset and correspond to large structural changes.

3.3. Rotation shear ramp

The flow curves of all samples were observed to have a good fit to the two models used for curve fitting with their correlation coefficients (R^2) greater than 0.99. The Casson model is a two-parameter model that is commonly used to predict the τ_y and μ_p of different types of materials more precisely at low shear rates (Herrada-Manchón et al., 2023). In this study, the plastic viscosity was observed to increase with the quantity of H added to the A gels whereas, it decreased after the addition of caffeine to the formulation. The μ_p however, stayed constant before again decreasing in the formulations containing undissolved caffeine (Fig. 6a & e). Roussel (2018) stated that the pressure required for printing is related to the τ_y and μ_p depending on whether the bulk material was pre-sheared or not before getting to the nozzle. Furthermore, when only the printing pressure is considered, the local pressure gradient (therefore, extrudability) is mostly related to the plastic viscosity of the printable material,and the contribution of yield stress could be neglected. We can thus, infer that a higher printing pressure would be required to extrude samples containing higher H, or the suspensions. However, since the 3D printer used in this study possessed both a pneumatic system as well as an extruder screw, the printing pressure would not only depend on the μ_p but also on the τ_y. Furthermore, high shape retention has been associated with the yield stress, and it can be used as an indirect indication of the ink's ability to support subsequent stacked layers (Bom et al., 2022).

It should be noted that the yield stress values determined by model fitting are frequently termed dynamic yield stresses and are defined as the minimum stress needed for maintaining flow, whereas the static yield stress is determined from the crossover point of a stress ramp measurement and is defined as the stress needed for initiating flow and is frequently higher in value (Malvern Instruments Limited, 2012; Qian & Kawashima, 2018). It is generally considered better to measure the static yield stress when looking at initiating flow in a material, like in the case of pushing the material through the feeding tube to the nozzle. The dynamic yield stress, on the other hand, is more suitable in applications involving stopping or maintaining flow after initiation, like in the case of shape retention after printing. Even though we were unable to measure the static stress of the samples in this study (no cross-over point was observed), interesting trends were observed from the estimation of the dynamic yield stress,τ_y. From Fig. 6b, the τ_y was observed to be mostly lower for AH gels than for pure gels (except for 4A2H) whereas for samples containing caffeine and sucrose (Fig. 6f), the yield stress was observed to increase with increasing caffeine concentration for

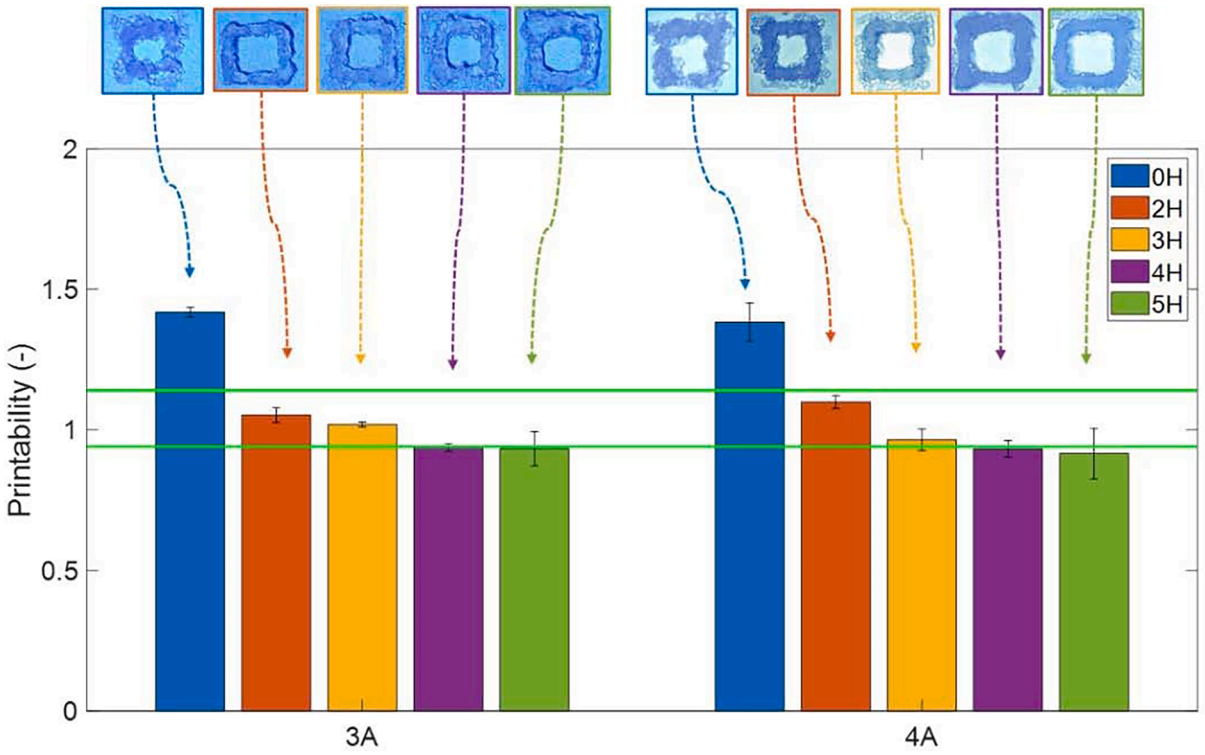

Fig. 7. Printability values of A and AH gels. Error bars are standard deviations based on four replicates.

formulations containing greater than 3 % of the model drug. Thus, concerning the pressure, τ_y and μ_p have opposite effects on the pressure with increase in HPMC and Caffeine. This antagonism could lead to a reduction or no difference in the printing pressure based on the magnitude of both parameters. In addition, higher values of these two parameters could result in better shape retention, but could also lead to poorer extrudability due to the need for higher extrusion force (or pressure) during printing (Martínez-Monzó et al., 2019; Zidan et al., 2019).

The Ostwald-de Waele, or Power-law model, is the most used mathematical model for describing the behaviour of pseudoplastic fluids because of its simplicity. While it is a good fit for fluids when measured at low shear rates, care should be taken with the parameters obtained from the model. The model assumes a non-linear relationship between the shear stress and the shear rate, it however, neglects the viscosity at rest and the viscosity as the shear rate approaches infinity. Nevertheless, it offers a good description of fluid behaviour across the range of shear rates to which the coefficients were fitted in this study (R^2 was greater than 0.9). As shown in Fig. 6c & g, all samples presented shear thinning properties ($n < 1$) that decreased with an increase in HPMC concentration and increased with the caffeine contained in the formulation. The consistency index of AH gels did not follow an obvious trend (Fig. 6d), whereas it increased with caffeine concentration (Fig. 6h). A high value of K has been used as an indication of the poor extrudability of mashed potatoes in the study by Liu et al., (2018) whereas a smaller value of n, indicates a more pronounced shear-thinning behaviour (Wilson et al., 2017). This shear-thinning ability makes materials extrudable since it allows the shear forces to align the macromolecules along the flow direction, thereby decreasing the viscosity (Bercea, 2023). Since the n and K are related to how easily materials are extruded through the printer's nozzle, samples containing HPMC, and caffeine might display poorer extrudability as highly viscous materials might block the nozzle and stick on the extruder walls. However, a higher consistency index could also mean the material possesses more mechanical strength to support extruded layers (Karyappa & Hashimoto, 2019).

3.4. Printability studies

From Fig. 7, it was observed that the A gels exhibited poor printability ($Pr > 1.14$), as evidenced by the deposition of irregular filaments during printing and the poor visual appearance of the printed shape. This could be due to their higher G', K and τ_y, thereby resulting in poor extrudability and hence poor printability. In contrast, AH gels had a statistically significant difference ($p < 0.05$) in printability when compared to the A gels. Their printability was found to be better ($Pr < 1.14$) with increasing HPMC concentration Thus, confirming our hypothesis that the addition of HPMC could improve the printability (extrudability) of agar gels. However, the addition of 4H and 5H resulted in the printability being less than 0.94. These samples had lower yield stresses when compared to the A gels, which could explain their poorer shape fidelities ($Pr < 0.94$). In general, 3D printing requires materials with low yield stress to make the material flow out of the nozzle, but if the yield stress is too low, the material collapses at the weight of added layers and thus, is not self-supporting. The lower Pr for A4H and A5H gels could also be because of their higher phase angles, resulting in squares with rounded corners that flowed over time and hence, poorer shape retention abilities. These samples were also very sticky and were difficult to remove from the printing plate, highlighting the need for post-processing. However, samples with intermediate rheological parameters, such as 3A2H, showed good extrudability and better shape retention capabilities. This could be due to its rheological property being within the acceptable range as reported by other studies (del-Mazo-Barbara & Ginebra, 2021; Karyappa & Hashimoto, 2019; Lille et al., 2018; Liu et al., 2018).

From Fig. 8, the 10S0C and formulations containing caffeine all displayed a Pr index that was within the acceptable range. Furthermore, the Pr of samples containing greater than 3C (suspensions) was

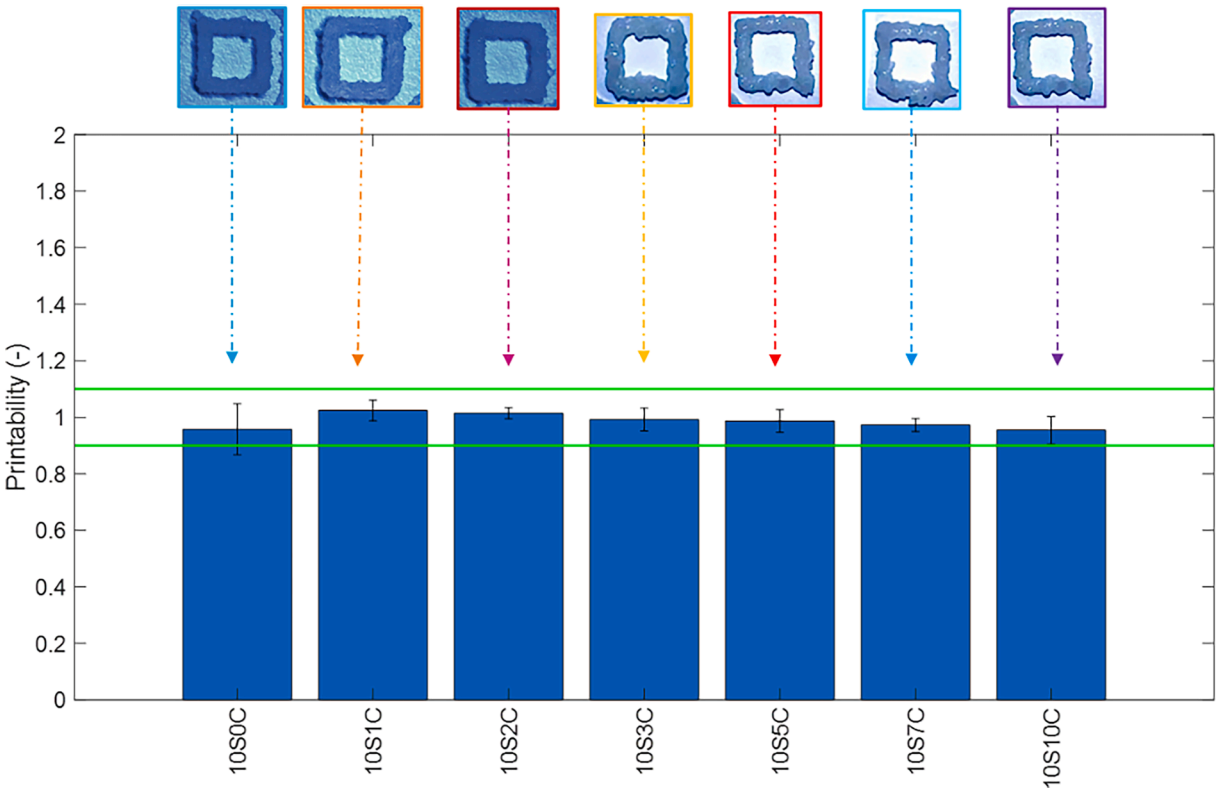

Fig. 8. Printability values of 10S gels of different caffeine concentrations. Error bars are standard deviations based on four replicates.

significantly different ($p < 0.05$) from samples containing 1C and 2C (gels). Other samples that had proper gelation ($0.94 < Pr < 1.14$) displayed intermediate G', τ_y and CEM values and especially, in the case of the suspensions containing undissolved caffeine, they displayed proper gelation even though they had remarkably high values of these 3 parameters. One would have expected that the samples containing greater than 3 % caffeine to be too hard to extrude and therefore have poor printability, but aside from the slight increase in pressure from 4 to 4.6 bar, all the samples displayed good extrudability as well as good shape retention. These findings demonstrate that τ_c at which the G' reduces rapidly as well as low values of n (as observed for the suspensions) result in good extrudability of otherwise hard-to-extrude samples. This observation further demonstrates that one rheological parameter alone is not capable of describing the behaviour of printed materials especially once they start flowing (Maldonado-Rosas et al., 2022) but instead, the gels appeared printable within a broad range of conditions i.e., at low τ_c and high τ_y. We would also like to state that although good extrudability and ductile deformation were observed at high CEM for the suspensions, this was not the case for A gels that showed brittle deformation and poor extrudability. We attributed the ductile extrusion of the suspensions to their higher phase angles. These high phase angles might translate to poor shape retention, but this was not the case because as already stated, the samples also possessed high G' and τ_y. There are thus, certain limits within which the rheological properties of a sample must exist, to facilitate both extrusion and shape retention (Corker et al., 2019).

It should also be highlighted that the extrusion of materials with high or low G′ is dependent on the type of printer used. For example, in the study by Lille et al., the authors reported that pastes with τ_y and G' greater than 20 and 1000 Pa, respectively, were able to retain the printed shape after extrusion. However, samples with τ_y and G' lesser than 10 and 300 Pa, respectively, could not retain the printed shape, and the samples with G′ greater than 36 kPa had poor extrudability (Lille et al., 2018). Indeed, it would have been difficult if not impossible to extrude the 10S10C formulation (thus, regarded as hard to extrude) for some printers like the one used by Lille et al., (2018). However, with the printer used in this study, we were able to achieve the extrusion due to the extrusion pressure being within the range of the materials requirement as well as the pre-shearing of the materials that was performed at the nozzle and before deposition. Certainly, this also means that materials that others have reported printable (Cheng et al., 2020), were considered to be unprintable using our 3D printer due to their low viscosity, yield stress and elastic modulus of the samples. Furthermore, there is also the matter of whether the material forms or not a lubrication layer during the feeding of the nozzle. For example, during a preliminary study using 12 % HPMC, we observed that the extrusion was only possible when the extruder screw was turned off. This could be because of the lubrication layer that was destroyed during the shearing and the laminar condition for shear localization thus not being fulfilled, thereby, leading to the loss of the plug flow zone that might otherwise be needed for the extrusion of the samples (Roussel, 2018). This further highlight that the dependence of printability is not only on the rheological properties but also on the specifications of the 3D printer used.

3.5. Correlation test

Performing 3D printing tests and evaluating the printability of samples can be time-consuming. It would be promising if these printability studies could be assessed more quickly using rheological tests and choose one or two pertinent rheological parameters that show strong correlations with printability. Several authors have sought to correlate rheological attributes to several print assessment criteria (Bom et al., 2022; Gao et al., 2018; Nadernezhad & Groll, 2022). For example, Gao et al., (2018) studied the effect of G', G'' and tan δ on the structural integrity and extrusion uniformity using alginate/gelatine-based gels. They concluded that G' and G" were related more to the printing pressure whereas tan δ correlated more with the shape fidelity and extrusion

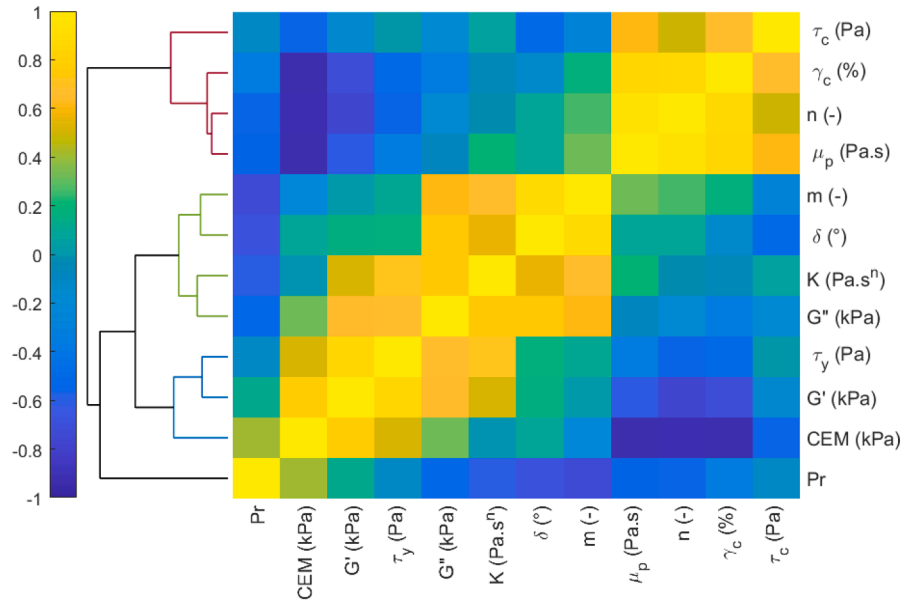

Fig. 9. Spearman rank-order correlation matrix and the linkage according to hierarchical cluster analysis of Spearman's correlations.

uniformity. Nadernezhad & Groll, (2022) also evaluated the print quality of formulations using rheological parameters, such as the G', tan δ, *K*, *n* and τ_y. Based on the Spearman rank-order correlation matrix and their linkage based on hierarchical cluster analysis, they identified that *K* and *n* belonged to the same cluster and described the ease of flow whereas, the other parameters belonged to the second cluster, describing the viscoelasticity of the formulations, their resistance against the flow and the extent of their viscous deformation afterwards. The model predicts that from a statistical point of view, a formulation becomes printable when it shows a high yield viscosity and a low degree of plasticity before the flow. Higher elastic materials also tended to be more printable when they possess more elasticity at a lower range of frequencies and a highly viscous nature at a higher range.

To the best of our knowledge, there have not been studies that correlated the semi-quantitative method to access printability, as developed by Ouyang et al., (2016), to rheological properties of gels intended for pharmaceutical purposes. We therefore sought to explore and understand the correlations between the rheological attributes of the seventeen samples studied as well as the correlation of their rheological attributes to their printability using Spearman rank-order correlation matrix and the linkage based on hierarchical cluster analysis of Spearman's correlations. From Fig. 9, three main clusters of features (red, green, and blue dendrograms) with distinct linkage distances from each other can be identified. The first cluster (in red) involves τ_c, γ_c, *n* and μ_p and they all describe correlations between the ease of the flow of the samples into the nozzle and the force requirements to sustain the flow during printing. The second cluster (in green) describes the homogeneity of the extrusion and the ability of the material to support its weight since it includes *m*, *δ*, K and G''. In this study, low values of these parameters were attributes of samples that showed over-gelation and had high printability. Since materials with good shape retention possess high τ_y and G' (thus, high CEM), the third cluster, describes the comportment after printing. Furthermore, regarding the monotonic relationship of the sample's rheological parameters to their printability,*m* and *δ* displayed the most significant monotonic relationship with *Pr* ($p < 0.05$).

3.6. Dimensionality reduction using principal component analysis

There exists little literature on the discrimination of 3D printing performance based on rheological data of gels containing pharmaceutical ingredients using PCA. For food products, there was however, a study by Liu et al., (2020) where PCA was used to classify attributes of mashed potatoes based on the G', G'', G*, K, and n. PC1 and PC2 respectively accounted for 97.90 and 1.59 % of the total variance. In their study, all the tested parameters were close to each other on the right side of the PC1 axis. In addition, the authors identified three clusters that were representative of the printing performance of the samples (evaluated in terms of achieved printing percentage). The first cluster corresponded to samples that were self-supporting but not extrudable and were at the very right of the score plot. The second cluster corresponded to samples that were self-supporting and extrudable and were in the middle of the score plot. The last cluster corresponded to samples that were extrudable but not self-supporting and were at the left of the score plot. The authors further indicated PCA to be a useful tool for identifying clusters based on samples' rheological properties and actual 3D printing performance (Liu et al., 2020).

Fig. 10 shows the loadings and score plot of the measured responses in space for the PCA analysis conducted in this study. Using Kaiser's rule, we kept the first three components since they had eigenvalues that were greater than 1. Like the study described above, there was a clear separation between the samples based on their printability. Principal Component 1 (PC 1) described parameters related to the mechanical strength of the formulation to hold the printed structures and the magnitude of force necessary to extrude samples. It corresponded to 55.8 % of the total sample variance; G', YS (τ_y), CEM, K, and G'' correlated positively with these axes whereas, YP (τ_c), γ_c, n and μ_p correlated negatively. Regarding PC 1, samples that had higher values of the rheological parameters (e.g. 10S10C) required higher extrusion force (or pressure) to print, whereas samples with lower values and requiring lower extrusion force, were at the bottom. Principal Component 2 (PC 2) corresponded to 26.2 % of the total variance, it described the ease of flow of the material and the viscosity during printing since μ_p, *δ*, *m*, γ_c, *K* and *n* were predominant on this axis. Samples that we classified as under-gelled (yellow markers) had higher values of these parameters, correlated more positively with PC 2, and were therefore at

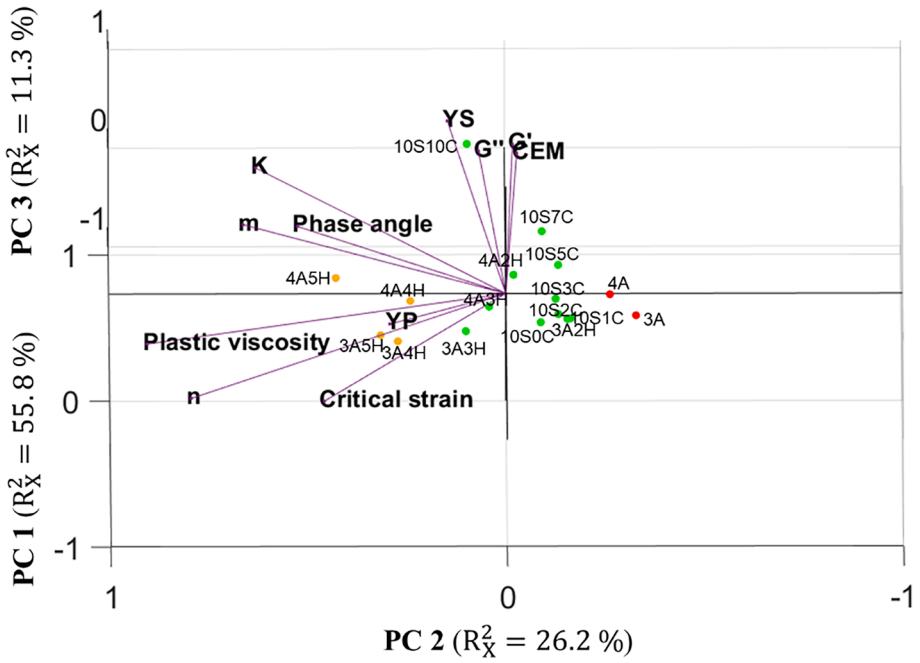

Fig. 10. PCA score and loading plot.

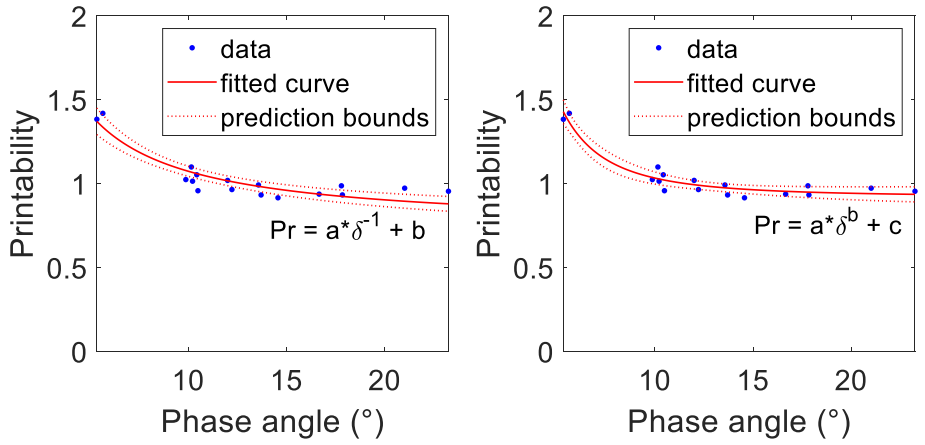

Fig. 11. Scatter plot of phase angle vs printability showing the fitted curves: (a) exponential model (b) power model and their prediction bounds.

the left. Though these under-gelled samples had good ductility they could, however, result in poor extrudability during printing due to their very viscous nature (high μ_p). Samples that were properly gelled and had intermediate values of the parameters that were predominant in PC 2 and were at the middle whereas, samples that were over-gelled and had the lowest values of all the samples were at the right. Lastly, principal component 3 (PC 3) corresponded to 11.3 % of the explained variance. K, YP (τ_c) and YS (τ_y)) were predominant in this axis. Higher values of these parameters have been correlated to improved mechanical strength to support extruded layers (Herrada-Manchón et al., 2023; Karyappa & Hashimoto, 2019; Mouser et al., 2016). Thus, PC 1 represented the extrusion force necessary to extrude the gels, PC 2 the sample's extrudability, and PC 3 the shape retention ability of the extruded samples. Furthermore, two parameters correlated with all three PCs: m and δ. Both parameters describe the relationship between the viscous and elastic parts of viscoelastic materials. It is therefore apt to see that they had correlations with the three PCs. Since a material that is too solid (low m and δ) would have good shape retention but would require higher extrusion force and display poor extrudability. Whereas a material that is too liquid (high m and δ), would display better extrudability and would require lower extrusion force but poor good shape retention.

3.7. Prediction of printability using regression models

The prediction of print quality (evaluated using the precision factor, the pressure needed for extrusion, shape fidelity, etc.) using rheological attributes has been reported in the literature (Ainis et al., 2023; Gao et al., 2018; Gillispie et al., 2023). These studies all highlight that one rheological parameter can designated as the primary physicochemical parameter affecting print quality, but it does not by itself reflect the complex behaviour of hydrogel-based inks during the 3D printing process. For example in the study by Gillispie et al., (2023), it was highlighted that the shape fidelity of samples with high tan δ would be underestimated if it was used to predict the shape fidelity. This is most likely due to a low tan δ being considered a good predictor for high shape fidelity whereas other parameters such as yield stress could also

Table 2
Prediction models for printability.

Regression model	Prediction Formula	R^2Y (%)	RPD (-)
Inverse linear	$3.322*\delta^{-1} + 0.744$	*84.71*	*2.48*
Power	$38.42*\delta^{-2.598} + 0.933$	*91.79*	*3.27*

contribute to a sample's shape fidelity. Ribeiro et al., (2017) also proposed a model using yield stress to predict filament deformation and estimate shape fidelity. However, Amorim et al., (2021) highlighted that the measurement of the yield stress alone is not an indicator of good printability instead, other parameters are needed to infer from this parameter. Nevertheless, we sought to further explore the prediction of the sample's printability using their rheological attributes(s). We have already ascertained from previous sections that m and δ both had statistically significant negative monotonic relationships with printability. We also showed the strong covariance (seen in the PCA model) between m and δ, which meant a near-equal regression model could be constructed with either of the parameters as independent variables. We therefore chose to model the printability using only the δ. R^2Y and RPD were used to evaluate the predictive performance of the two models selected.

The scatter plot of the data for the samples (Fig 11) shows the printability approaching an asymptote and was thus fitted in linear regression by including the reciprocal (1/X) of the phase angle in the model. Furthermore, since the *Pr* decreases as the phase angle increases (clusters observed at higher phase angle), the plots appear to also be compatible with a power-law model, approaching an asymptote somewhere around 1. The printability prediction equations as well as the evaluation parameters (R^2Y and RPD) of both models are presented in Table 2. R^2Y values greater than 0.83 were observed for both models and their RPD values were greater than 2.5, suggesting a good predictive performance of the exponential and power regression models of gel printability using the phase angle. It should be noted that the prediction power of the power regression model was superior to that of the inverse linear regression as indicated by the higher R^2Y and RPD. However, the estimation of the printability of samples with δ could be over or underestimated, so care should be taken with the use of the values obtained from using these models. Nevertheless, comparative values can be determined, and estimations of printability can be proposed using the models presented below.

4. Conclusion

The suitability of A and AH gels for 3D extrusion printing was investigated using their rheological properties and principal component analysis. Using principal component analysis, three components accounted for over 90 % of the variances of the rheological data and they were correlated to the extrudability, extrusion force, and shape fidelity of the samples. Furthermore, three clusters were highlighted according to the sample's printability, and we observed that adding HPMC contributed to the formulation extrudability, whereas agar and caffeine contributed to the shape retention. Although, adding the model drug, caffeine into the formulation resulted in higher G' and τ_0, the samples still demonstrated better extrudability due to the higher phase angles and the deviation from true gels to suspensions with paste-like texture. Furthermore, the regression models in this study provided a good prediction of the printability values using the phase angle. Thus, one rheological parameter would seem to be appropriate to characterize the printability of formulations for extrusion 3D printing. As a complement to this information, either the G' or the τ_y could be used to evaluate the sample's flow behaviour and mechanical strength. It should be noted that the estimated models are based on the 3D printing process parameters and the rheological measurements protocol and that no absolute printability values can be determined with the prediction models in general. Nevertheless, comparative values can be determined, and estimations of printability can be proposed with the models presented in this study. Further investigations and additional prediction models using other polymers and other printability measurements would need to be performed in the future to further confirm these results. In addition, an investigation of the different formulations on the drug release properties of the gels should be conducted to consider any possible effect on the dissolution properties of the drug matrix.

Funding

The authors are grateful to the Occitanie Region and ANR "Investissements d'Avenir" program, ANR-18-EURE-0021 project, for funding.

CRediT authorship contribution statement

Morenikeji Aina: Writing – review & editing, Writing – original draft, Methodology, Investigation, Data curation, Conceptualization. **Fabien Baillon:** Writing – review & editing, Visualization, Supervision, Software, Methodology. **Romain Sescousse:** Writing – review & editing, Supervision, Resources, Methodology, Investigation, Formal analysis. **Noelia M Sanchez-ballester:** Writing – review & editing, Supervision, Methodology, Investigation. **Sylvie Begu:** Writing – review & editing, Supervision, Resources, Project administration. **Ian Soulairol:** Writing – review & editing, Validation, Supervision, Resources, Formal analysis, Conceptualization. **Martial Sauceau:** Writing – review & editing, Validation, Supervision, Resources, Project administration, Funding acquisition, Formal analysis, Conceptualization.

Declaration of competing interest

The authors declare that they have no known competing financial interests or personal relationships that could have appeared to influence the work reported in this paper.

Data availability

Data will be made available on request.

References

Ainis, W.N., Feng, R., van den Berg, F.W.J., Ahrné, L., 2023. Comparing the rheological and 3D printing behavior of pea and soy protein isolate pastes. Innov. Food Sci. Emerg. Technol. 84, 103307 https://doi.org/10.1016/j.ifset.2023.103307.

Alqahtani, A.A., Ahmed, M.M., Mohammed, A.A., Ahmad, J., 2023. 3D printed Pharmaceutical Systems for Personalized Treatment in metabolic syndrome. Article 4 Pharmaceutics 15 (4). https://doi.org/10.3390/pharmaceutics15041152.

Amorim, P.A., d'Ávila, M.A., Anand, R., Moldenaers, P., Van Puyvelde, P., Bloemen, V., 2021. Insights on shear rheology of inks for extrusion-based 3D bioprinting. Bioprinting 22, e00129.

Baumgardner, G., Rowe, G., Rossiter, W., Wallace, T., Dean, S., 2007. Specifications for roofing and industrial asphalts using dynamic shear rheometry (DSR). J. ASTM Int. 4 https://doi.org/10.1520/JAI101044.

Bercea, M., 2023. Rheology as a tool for fine-tuning the properties of printable bioinspired gels. Molecules 28 (6), 2766. https://doi.org/10.3390/molecules28062766.

Bhutani, U., Basu, T., Majumdar, S., 2021. Oral drug delivery: conventional to long acting new-age designs. Eur. J. Pharm. Biopharm. 162, 23–42. https://doi.org/10.1016/j.ejpb.2021.02.008.

Bi, C., Wang, L.-J., Li, D., Huang, Z., Adhikari, B., Chen, X., 2017. Non-linear rheological properties of soy protein isolate dispersions and acid-induced gels. Int. J. Food Eng. 13 https://doi.org/10.1515/ijfe-2016-0167.

Bom, S., Ribeiro, R., Ribeiro, H.M., Santos, C., Marto, J., 2022. On the progress of hydrogel-based 3D printing: correlating rheological properties with printing behaviour. in. Int. J. Pharm. 615 https://doi.org/10.1016/j.ijpharm.2022.121506.

Boudriau, S., Hanzel, C., Massicotte, J., Sayegh, L., Wang, J., Lefebvre, M., 2016. Randomized comparative bioavailability of a novel three-dimensional printed fast-melt formulation of levetiracetam following the Administration of a Single 1000-mg dose to healthy human volunteers under fasting and fed conditions. Drugs R&D 16 (2), 229–238. https://doi.org/10.1007/s40268-016-0132-1.

Cailleaux, S., Sanchez-Ballester, N.M., Gueche, Y.A., Bataille, B., Soulairol, I., 2021. Fused deposition modeling (FDM), the new asset for the production of tailored medicines. J. Control. Release 330, 821–841. https://doi.org/10.1016/j.jconrel.2020.10.056.

Cheng, Y., Qin, H., Acevedo, N.C., Jiang, X., Shi, X., 2020. 3D printing of extended-release tablets of theophylline using hydroxypropyl methylcellulose (HPMC) hydrogels. in. Int. J. Pharm. 591 https://doi.org/10.1016/j.ijpharm.2020.119983.
Cheng, Y., Fu, Y., Ma, L., Yap, P.L., Losic, D., Wang, H., Zhang, Y., 2022. Rheology of edible food inks from 2D/3D/4D printing, and its role in future 5D/6D printing. Food Hydrocoll. 132, 107855 https://doi.org/10.1016/j.foodhyd.2022.107855.
Chile, L.-E., Mehrkhodavandi, P., Hatzikiriakos, S., 2017. Aromatic interactions in aryl-capped polylactides: a thermorheological investigation. J. Rheol. 61, 1137–1148. https://doi.org/10.1122/1.5000804.
Cofelice, M., Messia, M.C., Marconi, E., Cuomo, F., Lopez, F., 2023. Effect of the xanthan gum on the rheological properties of alginate hydrogels. Food Hydrocoll. 142, 108768 https://doi.org/10.1016/j.foodhyd.2023.108768.
Corker, A., Ng, H., Poole, R., García-Tuñón, E., 2019. 3D printing with 2D colloids: designing rheology protocols to predict 'printability' of soft-materials. Soft Matter 15. https://doi.org/10.1039/C8SM01936C.
Deb, P.K., Abed, S.N., Jaber, A.M.Y., Tekade, R.K., 2018. Chapter 5—Particulate level properties and its implications on product performance and processing. In: Tekade, R.K. (Ed.), Dosage Form Design Parameters. Academic Press, pp. 155–220. https://doi.org/10.1016/B978-0-12-814421-3.00005-1.
del-Mazo-Barbara, L., Ginebra, M.P., 2021. Rheological characterisation of ceramic inks for 3D direct ink writing: a review. J. Eur. Ceram. Soc. 41 (16), 18–33. https://doi.org/10.1016/j.jeurceramsoc.2021.08.031.
Dille, M. J., Draget, K. I., & Hattrem, M. N. (2015). The effect of filler particles on the texture of food gels. In *Modifying Food Texture: Novel Ingredients and Processing Techniques* (pp. 183–200). Scopus. https://doi.org/10.1016/B978-1-78242-333-1.00009-7.
dos Santos, J., Balbinot, G. de S., Buchner, S., Collares, F.M., Windbergs, M., Deon, M., Beck, R.C.R., 2023. 3D printed matrix solid forms: can the drug solubility and dose customisation affect their controlled release behaviour? Int. J. Pharmaceutics: X 5, 100153. https://doi.org/10.1016/j.ijpx.2022.100153.
El Bitouri, Y., 2023. Rheological behavior of cement paste: a phenomenological state of the art. Eng 4 (3), Article 3. https://doi.org/10.3390/eng4030107.
Elbadawi, M., Gustaffson, T., Gaisford, S., Basit, A.W., 2020. 3D printing tablets: predicting printability and drug dissolution from rheological data. Int. J. Pharm. 590, 119868 https://doi.org/10.1016/j.ijpharm.2020.119868.
Feroz, S., Dias, G., 2021. Hydroxypropylmethyl cellulose (HPMC) crosslinked keratin/hydroxyapatite (HA) scaffold fabrication, characterization and in vitro biocompatibility assessment as a bone graft for alveolar bone regeneration. Heliyon 7 (11), e08294.
Firth, J., Basit, A. W., & Gaisford, S. (2018). The Role of Semi-Solid Extrusion Printing in Clinical Practice. In A. Basit & S. Gaisford (Eds.), *3D Printing of Pharmaceuticals* (Vol. 31, pp. 133–151). https://doi.org/10.1007/978-3-319-90755-0_7.
Gao, T., Gillispie, G.J., Copus, J.S., Asari, A.K.P.R., Seol, Y.-J., Atala, A., Yoo, J.J., Lee, S. J., 2018. Optimization of gelatin-alginate composite bioink printability using rheological parameters: a systematic approach. Biofabrication 10 (3), 034106. https://doi.org/10.1088/1758-5090/aacdc7.
Genovese, D.B., Lozano, J.E., Rao, M.A., 2007. The rheology of colloidal and noncolloidal food dispersions. J. Food Sci. 72 (2), R11–R20. https://doi.org/10.1111/j.1750-3841.2006.00253.x.
Georgopoulos, T., Larsson, H., Eliasson, A.-C., 2004. A comparison of the rheological properties of wheat flour dough and its gluten prepared by ultracentrifugation. Food Hydrocoll. 18 (1), 143–151. https://doi.org/10.1016/S0268-005X(03)00059-6.
GhavamiNejad, A., Ashammakhi, N., Wu, X.Y., Khademhosseini, A., 2020. Crosslinking strategies for three-dimensional bioprinting of polymeric hydrogels. Small 16 (35), e2002931.
Gholamipour-Shirazi, A., Norton, I.T., Mills, T., 2019. Designing hydrocolloid based food-ink formulations for extrusion 3D printing. Food Hydrocoll. 95, 161–167. https://doi.org/10.1016/j.foodhyd.2019.04.011.
Gillispie, G.J., Copus, J., Uzun-Per, M., Yoo, J.J., Atala, A., Niazi, M.K.K., Lee, S.J., 2023. The correlation between rheological properties and extrusion-based printability in bioink artifact quantification. Mater. Des. 233, 112237 https://doi.org/10.1016/j.matdes.2023.112237.
Gu, S., Cheng, G., Yang, T., Ren, X., Gao, G., 2017. Mechanical and rheological behavior of hybrid cross-linked polyacrylamide/cationic micelle hydrogels. Macromol. Mater. Eng. 302 (12), 1700402. https://doi.org/10.1002/mame.201700402.
Heckl, M.P., Korber, M., Jekle, M., Becker, T., 2023. Relation between deformation and relaxation of hydrocolloids-starch based bio-inks and 3D printing accuracy. Food Hydrocoll. 137, 108326 https://doi.org/10.1016/j.foodhyd.2022.108326.
Herrada-Manchón, H., Rodríguez-González, D., Fernández, M.A., Kucko, N.W., Barrère-de Groot, F., Aguilar, E., 2022. Effect on rheological properties and 3D printability of biphasic calcium phosphate microporous particles in hydrocolloid-based hydrogels. Gels 8 (1), 28. https://doi.org/10.3390/gels8010028.
Herrada-Manchón, H., Fernández, M.A., Aguilar, E., 2023. Essential guide to hydrogel rheology in extrusion 3D printing: how to measure it and why it matters? gels, 9(7). Article 7. https://doi.org/10.3390/gels9070517.
Herrada-Manchon, H., Rodriguez-Gonzalez, D., Fernandez, M.A., Sune-Pou, M., Perez-Lozano, P., Garcia-Montoya, E., Aguilar, E., 2020. 3D printed gummies: personalized drug dosage in a safe and appealing way. in. Int. J. Pharm. 587 https://doi.org/10.1016/j.ijpharm.2020.119687.
Hsiao, W.-K., Lorber, B., Paudel, A., 2020. Can 3D printing of oral drugs help fight the current COVID-19 pandemic (and similar crisis in the future)? Expert Opin. Drug Deliv. 17 (7), 899–902. https://doi.org/10.1080/17425247.2020.1772229.
Hyun, K., Kim, S.H., Ahn, K.H., Lee, S.J., 2002. Large amplitude oscillatory shear as a way to classify the complex fluids. J. Nonnewton. Fluid Mech. 107 (1), 51–65. https://doi.org/10.1016/S0377-0257(02)00141-6.
TA Instruments. (n.d.). *How to Improve Additive Manufacturing (3D printing) with Rheology*. Retrieved 1 May 2023, from https://www.tainstruments.com/how-to-improve-additive-manufacturing-3d-printing-with-rheology/.
Jeong, B., Kim, S.W., Bae, Y.H., 2012. Thermosensitive sol–gel reversible hydrogels. Adv. Drug Deliv. Rev. 64, 154–162. https://doi.org/10.1016/j.addr.2012.09.012.
Joshi, S.C., 2011. Sol-gel behavior of hydroxypropyl methylcellulose (HPMC) in ionic media including drug release. Materials 4 (10), 1861–1905. https://doi.org/10.3390/ma4101861.
Kamlow, M.-A., Vadodaria, S., Gholamipour-Shirazi, A., Spyropoulos, F., Mills, T., 2021. 3D printing of edible hydrogels containing thiamine and their comparison to cast gels. Food Hydrocoll. 116, 106550 https://doi.org/10.1016/j.foodhyd.2020.106550.
Karavasili, C., Zgouro, P., Manousi, N., Lazaridou, A., Zacharis, C.K., Bouropoulos, N., Moschakis, T., Fatouros, D.G., 2022. Cereal-based 3D printed dosage forms for drug administration during breakfast in pediatric patients within a hospital setting. J. Pharm. Sci. 111 (9), 2562–2570. https://doi.org/10.1016/j.xphs.2022.04.013.
Karyappa, R., Hashimoto, M., 2019. Chocolate-based ink three-dimensional printing (Ci3DP). Sci. Rep. 9 (1), 14178. https://doi.org/10.1038/s41598-019-50583-5.
Klost, M., Brzeski, C., Drusch, S., 2020. Effect of protein aggregation on rheological properties of pea protein gels. Food Hydrocoll. 108, 106036 https://doi.org/10.1016/j.foodhyd.2020.106036.
Lille, M., Nurmela, A., Nordlund, E., Metsä-Kortelainen, S., Sozer, N., 2018. Applicability of protein and fiber-rich food materials in extrusion-based 3D printing. J. Food Eng. 220, 20–27. https://doi.org/10.1016/j.jfoodeng.2017.04.034.
Liu, S.Q., Joshi, S.C., Lam, Y.C., Tam, K.C., 2008. Thermoreversible gelation of hydroxypropylmethylcellulose in simulated body fluids. Carbohydr. Polym. 72 (1), 133–143. https://doi.org/10.1016/j.carbpol.2007.07.040.
Liu, Y., Yu, Y., Liu, C., Regenstein, J.M., Liu, X., Zhou, P., 2019. Rheological and mechanical behavior of milk protein composite gel for extrusion-based 3D food printing. LWT 102, 338–346. https://doi.org/10.1016/j.lwt.2018.12.053.
Liu, Z., Zhang, M., Bhandari, B., Yang, C., 2018. Impact of rheological properties of mashed potatoes on 3D printing. J. Food Eng. 220, 76–82. https://doi.org/10.1016/j.jfoodeng.2017.04.017.
Liu, Z., Zhang, M., Ye, Y., 2020. Indirect prediction of 3D printability of mashed potatoes based on LF-NMR measurements. J. Food Eng. 287, 110137 https://doi.org/10.1016/j.jfoodeng.2020.110137.
Lizarraga, M., Piantevicin, D., Gonzalez, R., Rubiolo, A., Santiago, L., 2006. Rheological behaviour of whey protein concentrate and λ-carrageenan aqueous mixtures. Food Hydrocoll. 20 (5), 740–748. https://doi.org/10.1016/j.foodhyd.2005.07.007.
Maldonado-Rosas, R., Tejada-Ortigoza, V., Cuan-Urquizo, E., Mendoza-Cachú, D., Morales-de la Peña, M., Alvarado-Orozco, J.M., Campanella, O.H., 2022. Evaluation of rheology and printability of 3D printing nutritious food with complex formulations. Addit. Manuf. 58, 103030 https://doi.org/10.1016/j.addma.2022.103030.
Malvern Instruments Limited. (2012). *Understanding yield stress measurements*. https://www.atascientific.com.au/wp-content/uploads/2017/02/MRK1782-01.pdf.
Mao, B., Bentaleb, A., Louerat, F., Divoux, T., Snabre, P., 2017. Heat-induced aging of agar solutions: impact on the structural and mechanical properties of agar gels. Food Hydrocoll. 64, 59–69. https://doi.org/10.1016/j.foodhyd.2016.10.020.
Mao, B., Bentaleb, A., Louerat, F., Divoux, T., & Snabre, P. (2016). Overcooked agar solutions: Impact on the structural and mechanical properties of agar gels. *arXiv: 1603.00778 [Cond-Mat]*. http://arxiv.org/abs/1603.00778.
Martínez-Monzó, J., Cárdenas, J., García-Segovia, P., 2019. Effect of temperature on 3D printing of commercial potato puree. Food Biophys. 14 (3), 225–234. https://doi.org/10.1007/s11483-019-09576-0.
Miller, J.A., Fredrickson, M.E., Greene, J.M., Jay, M., Oyewumi, M.O., 2022. Reimagining drug manufacturing paradigm in today's pharmacy landscape. J. Am. Pharm. Assoc. 62 (6), 1761–1764. https://doi.org/10.1016/j.japh.2022.08.024.
Mora-Castaño, G., Millán-Jiménez, M., Linares, V., Caraballo, I., 2022. Assessment of the extrusion process and printability of suspension-type drug-loaded AffinisolTM filaments for 3D printing. Article 4 Pharmaceutics 14 (4). https://doi.org/10.3390/pharmaceutics14040871.
Mouser, V.H.M., Melchels, F.P.W., Visser, J., Dhert, W.J.A., Gawlitta, D., Malda, J., 2016. Yield stress determines bioprintability of hydrogels based on gelatin-methacryloyl and gellan gum for cartilage bioprinting. Biofabrication 8 (3), 035003. https://doi.org/10.1088/1758-5090/8/3/035003.
Mu, R., Wang, B., Lv, W., Yu, J., Li, G., 2023. Improvement of extrudability and self-support of emulsion-filled starch gel for 3D printing: increasing oil content. Carbohydr. Polym. 301, 120293 https://doi.org/10.1016/j.carbpol.2022.120293.
Nadernezhad, A., Groll, J., 2022. Machine learning reveals a general understanding of printability in formulations based on rheology additives. Adv. Sci. 9 (29), 2202638. https://doi.org/10.1002/advs.202202638.
Nasu, A., Otsubo, Y., 2006. Rheology and UV protection properties of suspensions of fine titanium dioxides in a silicone oil. J. Colloid Interface Sci. 296 (2), 558–564. https://doi.org/10.1016/j.jcis.2005.09.036.
Nobile, M.R., Pirozzi, V., Somma, E., Gomez D'Ayala, G., Laurienzo, P., 2008. Development and rheological investigation of novel alginate/N-succinylchitosan hydrogels. J Polym Sci B 46 (12), 1167–1182. https://doi.org/10.1002/polb.21450.
Onsawai, P., Phetpan, K., Khurnpoon, L., Sirisomboon, P., 2021. Evaluation of physiological properties and texture traits of durian pulp using near-infrared spectra of the pulp and intact fruit. Measurement 174, 108684. https://doi.org/10.1016/j.measurement.2020.108684.
Ouyang, L., Yao, R., Zhao, Y., Sun, W., 2016. Effect of bioink properties on printability and cell viability for 3D bioplotting of embryonic stem cells. Biofabrication 8 (3), 035020. https://doi.org/10.1088/1758-5090/8/3/035020.

Anton Paar. (n.d.). *Amplitude sweeps*. Anton Paar Wiki. Retrieved 15 October 2023, from https://wiki.anton-paar.com/en/amplitude-sweeps/.

Panraksa, P., Zhang, B., Rachtanapun, P., Jantanasakulwong, K., Qi, S., Jantrawut, P., 2022. 'Tablet-in-syringe': a novel dosing mechanism for dysphagic patients containing fast-disintegrating tablets fabricated using semisolid extrusion 3D printing. Pharmaceutics 14 (2), 443. https://doi.org/10.3390/pharmaceutics14020443.

Perez-Robles, S., Carotenuto, C., Minale, M., 2022. HPMC hydrogel formation mechanisms unveiled by the evaluation of the activation energy. Polymers 14 (3), 635. https://doi.org/10.3390/polym14030635.

Polamaplly, P., Cheng, Y., Shi, X., Manikandan, K., Kremer, G.E., Qin, H., 2019. 3D printing and characterization of hydroxypropyl methylcellulose and methylcellulose for biodegradable support structures. Procedia Manuf. 34, 552–559. https://doi.org/10.1016/j.promfg.2019.06.219.

Qian, Y., Kawashima, S., 2018. Distinguishing dynamic and static yield stress of fresh cement mortars through thixotropy. Cem. Concr. Compos. 86, 288–296. https://doi.org/10.1016/j.cemconcomp.2017.11.019.

Rahman, J.M.H., Shiblee, M.N.I., Ahmed, K., Khosla, A., Kawakami, M., Furukawa, H., 2020. Rheological and mechanical properties of edible gel materials for 3D food printing technology. Heliyon 6 (12), e05859.

Rheology Testing Services. (n.d.). *Frequency Sweep | Rheology Testing Services | Chapel Hill, North Carolina*. Rheology Testing. Retrieved 2 May 2023, from https://www.rheologytestingservices.com/frequency-sweep.

Ribeiro, A., Blokzijl, M.M., Levato, R., Visser, C.W., Castilho, M., Hennink, W.E., Vermonden, T., Malda, J., 2017. Assessing bioink shape fidelity to aid material development in 3D bioprinting. Biofabrication 10 (1), 014102. https://doi.org/10.1088/1758-5090/aa90e2.

Roussel, N., 2018. Rheological requirements for printable concretes. Cem. Concr. Res. 112, 76–85. https://doi.org/10.1016/j.cemconres.2018.04.005.

Shen, Y., Lin, L., Wei, S., Yan, J., Xu, T., 2022. Research on the preparation and mechanical properties of solidified 3D printed concrete materials. Article 12 Buildings 12 (12). https://doi.org/10.3390/buildings12122264.

Sim, H.G., Ahn, K.H., Lee, S.J., 2003. Large amplitude oscillatory shear behavior of complex fluids investigated by a network model: a guideline for classification. J. Nonnewton. Fluid Mech. 112 (2), 237–250. https://doi.org/10.1016/S0377-0257(03)00102-2.

Spiller, G. (Ed.). (1997). Introduction to the Chemistry, isolation, and biosynthesis of methylxanthines. In S. M. Tarka & W. J. Hurst, *Caffeine*. CRC Press. https://doi.org/10.1201/9781420050134.

Tabriz, A.G., Mithu, M.S., Antonijevic, M.D., Vilain, L., Derrar, Y., Grau, C., Morales, A., Katsamenis, O.L., Douroumis, D., 2023. 3D printing of LEGO® like designs with tailored release profiles for treatment of sleep disorder. Int. J. Pharm. 632, 122574 https://doi.org/10.1016/j.ijpharm.2022.122574.

Tagami, T., Yoshimura, N., Goto, E., Noda, T., & Ozeki, T. (2019). *Fabrication of mucoadhesive oral films by the 3D printing of hydroxypropyl methylcellulose-based catechin-loaded formulations* (Vol. 42, Issue 11, pp. 1898–1905). Pharmaceutical Society of Japan. https://doi.org/10.1248/bpb.b19-00481.

Tang, W.-L., Tang, W.-H., Chen, W.C., Diako, C., Ross, C.F., Li, S.-D., 2017. Development of a rapidly dissolvable Oral pediatric formulation for mefloquine using liposomes. Mol. Pharm. 14 (6), 1969–1979. https://doi.org/10.1021/acs.molpharmaceut.7b00077.

Tejada-Ortigoza, V., Cuan-Urquizo, E., 2022. Towards the development of 3D-printed food: a rheological and mechanical approach. Foods 11 (9), 1191. https://doi.org/10.3390/foods11091191.

Temirel, M., Dabbagh, S.R., Tasoglu, S., 2022. Shape Fidelity evaluation of alginate-based hydrogels through extrusion-based bioprinting. *journal of functional*. Biomaterials 13 (4), Scopus. https://doi.org/10.3390/jfb13040225.

Teoh, X.-Y., Zhang, B., Belton, P., Chan, S.-Y., Qi, S., 2022. The effects of solid particle containing inks on the printing quality of porous pharmaceutical structures fabricated by 3D semi-solid extrusion printing. Pharm. Res. 39 (6), 1267–1279. https://doi.org/10.1007/s11095-022-03299-7.

Townsend, J.M., Beck, E.C., Gehrke, S.H., Berkland, C.J., Detamore, M.S., 2019. Flow behavior prior to crosslinking: the need for precursor rheology for placement of hydrogels in medical applications and for 3D bioprinting. Prog. Polym. Sci. 91, 126–140. https://doi.org/10.1016/j.progpolymsci.2019.01.003.

Tracy, T., Wu, L., Liu, X., Cheng, S., Li, X., 2023. 3D printing: innovative solutions for patients and pharmaceutical industry. Int. J. Pharm. 631, 122480 https://doi.org/10.1016/j.ijpharm.2022.122480.

Vandevivere, L., Denduyver, P., Portier, C., Häusler, O., De Beer, T., Vervaet, C., Vanhoorne, V., 2020. Influence of binder attributes on binder effectiveness in a continuous twin screw wet granulation process via wet and dry binder addition. Int. J. Pharm. 585, 119466 https://doi.org/10.1016/j.ijpharm.2020.119466.

Varges, P.M., Costa, C.S., Fonseca, B.F., Naccache, M., De Souza Mendes, P.R., 2019. Rheological characterization of carbopol® dispersions in water and in water/glycerol solutions. Article 1 Fluids 4 (1). https://doi.org/10.3390/fluids4010003.

Wang, J., Liu, Y., Zhang, X., Rahman, S.E., Su, S., Wei, J., Ning, F., Hu, Z., Martínez-Zaguilán, R., Sennoune, S.R., Cong, W., Christopher, G., Zhang, K., Qiu, J., 2021. 3D printed agar/ calcium alginate hydrogels with high shape fidelity and tailorable mechanical properties. Polymer 214, 123238. https://doi.org/10.1016/j.polymer.2020.123238.

Wei, J., Wang, J., Su, S., Wang, S., Qiu, J., Zhang, Z., Christopher, G., Ning, F., Cong, W., 2015. 3D printing of extremely tough hydrogel. RSC Adv. 5 https://doi.org/10.1039/C5RA16362E.

Wilson, S.A., Cross, L.M., Peak, C.W., Gaharwar, A.K., 2017. Shear-thinning and thermo-reversible nanoengineered inks for 3D bioprinting. ACS Appl. Mater. Interfaces 9 (50), 43449–43458. https://doi.org/10.1021/acsami.7b13602.

Yang, D., Gao, S., Yang, H., 2020. Effects of sucrose addition on the rheology and structure of iota-carrageenan. Food Hydrocoll. 99, 105317 https://doi.org/10.1016/j.foodhyd.2019.105317.

Yang, H.S., Kim, D.W., 2023. Fabrication of gastro-floating famotidine tablets: hydroxypropyl methylcellulose-based semisolid extrusion 3D printing. Pharmaceutics 15 (2), Article 2. https://doi.org/10.3390/pharmaceutics15020316.

Zhu, Y., Di, W., Song, M., Chitrakar, B., Liu, Z., 2023. Correlating 3D printing performance with sol-gel transition based on thermo-responsive k-carrageenan affected by fructose. J. Food Eng. 340, 111316 https://doi.org/10.1016/j.jfoodeng.2022.111316.

Zidan, A., Alayoubi, A., Coburn, J., Asfari, S., Ghammraoui, B., Cruz, C.N., Ashraf, M., 2019. Extrudability analysis of drug loaded pastes for 3D printing of modified release tablets. Int. J. Pharm. 554, 292–301. https://doi.org/10.1016/j.ijpharm.2018.11.025.